Biomaterials 30 (2009) 2523–2530

Contents lists available at ScienceDirect

Biomaterials

journal homepage: www.elsevier.com/locate/biomaterials

# Self-assembled peptide-based hydrogels as scaffolds for anchorage-dependent cells

Mi Zhou [a], Andrew M. Smith [a,b], Apurba K. Das [a,b,d], Nigel W. Hodson [c], Richard F. Collins [b], Rein V. Ulijn [a,b,d,*], Julie E. Gough [a,**]

[a] Materials Science Centre, School of Materials, The University of Manchester, Grosvenor Street, Manchester M1 7HS, UK
[b] Manchester Interdisciplinary Biocentre, The University of Manchester, Princess Street, Manchester M1 7ND, UK
[c] The University of Manchester, Oxford Road, Manchester M13 9PT, UK
[d] Department of Pure and Applied Chemistry/WestCHEM, University of Strathclyde, Cathedral Street, Glasgow G1 1XL, UK

ARTICLE INFO

*Article history:*
Received 24 October 2008
Accepted 6 January 2009
Available online 7 February 2009

*Keywords:*
Minimalist design
Self-assembly
Biomimetic materials
RGD ligands
3D culture
Anchorage-dependent cells

ABSTRACT

We report here the design of a biomimetic nanofibrous hydrogel as a 3D-scaffold for anchorage-dependent cells. The peptide-based bioactive hydrogel is formed through molecular self-assembly and the building blocks are a mixture of two aromatic short peptide derivatives: Fmoc-FF (Fluorenylmethoxycarbonyl-diphenylalanine) and Fmoc-RGD (arginine-glycine-aspartate) as the simplest self-assembling moieties reported so far for the construction of small-molecule-based bioactive hydrogels. This hydrogel provides a highly hydrated, stiff and nanofibrous hydrogel network that uniquely presents bioactive ligands at the fibre surface; therefore it mimics certain essential features of the extracellular matrix. The RGD sequence as part of the Fmoc-RGD building block plays a dual role of a structural component and a biological ligand. Spectroscopic and imaging analysis using CD, FTIR, fluorescence, TEM and AFM confirmed that FF and RGD peptide sequences self-assemble into β-sheets interlocked by π–π stacking of the Fmoc groups. This generates the cylindrical nanofibres interwoven within the hydrogel with the presence of RGDs in tunable densities on the fibre surfaces. This rapid gelling material was observed to promote adhesion of encapsulated dermal fibroblasts through specific RGD–integrin binding, with subsequent cell spreading and proliferation; therefore it may offer an economical model scaffold to 3D-culture other anchorage-dependent cells for *in-vitro* tissue regeneration.



## 1. Introduction

A major challenge in the design of new biomaterials is to exploit the versatility of biology while keeping systems simple, cheap, robust and reproducible. A key objective in this context is the design of extracellular matrix (ECM) mimics, providing the essential characteristics of a natural ECM in its ability to direct and control cell behaviour, yet with minimal complexity. Here we report the development of a biomimetic scaffold for 3D culture of anchorage-dependent cells with three-fold novelty: (i) its unique supramolecular architecture allows bioactive peptides to be presented at the surface of the nanofibres, similar to the peptides' orientation in natural ECM; (ii) the building blocks are simple and act simultaneously as structural and functional components; (iii) the hydrogel has been applied successfully in 3D culture of anchorage dependent HDFa (human adult dermal fibroblast) cells.

In natural extracellular matrix a plethora of complex biomolecules exist within the 3D-network of interlaced protein-nanofibres to communicate with resident cells [1]. One approach to mimicking natural ECM is the development of hydrogels through molecular self-assembly of peptides and their derivatives; these hydrogels comprise nanofibrous networks which imitate the structural architecture of ECM [2–10]. In order to incorporate biologically-active components, the termini of certain oligopeptide derivatives may be modified with bioactive ligands and upon assembly these groups are usually presented as flexible pendant groups [11–14].

One commonly exploited bioactive ligand is the tri-peptide sequence of RGD which was identified in the early 1980s within the hydrophilic loop of fibronectin as an independent cell attachment site [15]. It binds to transmembrane integrins which are cell-surface receptors and forms linkages coupling the ECM with the

* Corresponding author. Tel.: +44 141 548 2110; fax: +44 141 548 4822.
** Corresponding author. Tel.: +44 161 306 8958; fax: +44 161 306 3586.
*E-mail addresses:* rein.ulijn@strath.ac.uk (R.V. Ulijn), j.gough@manchester.ac.uk (J.E. Gough).

0142-9612/$ – see front matter © 2009 Elsevier Ltd. All rights reserved.
doi:10.1016/j.biomaterials.2009.01.010

cytoskeleton. As a prerequisite to the regulation of cell behaviour within a scaffold, cell adhesion is often promoted by introducing the RGD ligand into polymeric or supramolecular substrates [12,14,16–19]. Critical density and lateral spacing of the incorporated RGD ligands were demonstrated as vital for the enhancement of cell adhesion [20,21]. Ligand arrangement and configuration further influence the extent of cell adhesion where RGD clusters and cyclic RGDs were adopted [14,22].

In this work, we have adopted a 'minimalist approach' to use Fmoc-protected di/tri-peptides instead of longer peptides and derivatives [4–8,10–14,19], for the fabrication of self-assembled scaffolds that possess bioactivity. Our previous report on Fmoc-FF demonstrated its ability to self-assemble into nanofibres and form macroscopic hydrogels at neutral pH [9]. Based on the molecular architecture that we recently proposed for the self-assembled Fmoc-FF nanofibres [23], we sought to incorporate bioactive ligands through the same self-assembly mechanism giving rise to a next generation of Fmoc-peptide hydrogels which are bioactive. Since Fmoc-FF self-assembles under physiological conditions (pH 7.0 and 37 °C) [9], it offers a stable structural component to mix with Fmoc-RGD for the formation of hydrogels suitable as cell scaffolds. The unique molecular architecture was confirmed by various imaging and spectroscopic techniques and visco-elasticity was measured using a rheometer. Human dermal fibroblasts were cultured in 3D within the gels and analysed for viability and morphology using a live/dead assay, F-actin staining and a proliferation/viability assay. Integrin binding to the RGD ligands was determined using an integrin blocking antibody. Cell responses to the RGD gels were compared to gels containing RGE (a chemical analogue of RGD but does not promote cell adhesion [15]).

## 2. Materials and methods

### 2.1. Hydrogel preparation

Purity of Fmoc-FF (Bachem, Germany), Fmoc-RGD (Synthetech, USA), and Fmoc-RGE (Synthetech, USA) was measured to be >99.5% using high performance liquid chromatography (HPLC) and mass spectroscopy (MS) (as shown in Supplementary data, S1–S6). To prepare an aqueous solution of 10–20 mM Fmoc-FF, 2 mL distilled water ($dH_2O$, Gibco, UK) were pipetted into a 10 mL glass-vial which contained 0.0107–0.0214 g of Fmoc-FF. 0.5 M sodium hydroxide (NaOH, Fisher, UK) solution was added to the suspension to adjust pH to 10.0; alternating vortex and ultra-sonication were applied until a clear solution was obtained. This solution was then neutralized to pH = 7.2 by a dropwise addition of 0.5 M hydrochloric acid (HCl, Aldrich, UK) and kept at 20 or 37 °C for gelation. To prepare an aqueous solution of 10–20 mM Fmoc-RGD or Fmoc-RGE, 2 mL $dH_2O$ were added into a glass-vial with 0.0228 g of Fmoc-RGD or 0.0232 g Fmoc-RGE and 0.5 HCl solution was added dropwise to adjust pH to 3.0. Continuous ultra-sonication was applied until a transparent solution was formed and the solution was kept at 4 or 20 °C for gelation. To prepare mixed Fmoc-FF/RGD or Fmoc-FF/RGE solutions, 20 mM Fmoc-FF at pH 10.0 and 20 mM Fmoc-RGD (Fmoc-RGE) at pH 3 were mixed in various volume ratios within a 10 mL glass-vial and vortex was applied until the mixture appeared homogeneous. The mixed solution was further neutralized to pH 7.0 with dropwise addition of 0.5 M HCl or NaOH and kept at 37 °C for gelation with/without the addition of an equal volume of DMEM.

### 2.2. Atomic force microscopy

The morphology and width of the nanofibres within the self-assembled hydrogels were investigated using a Veeco Multimode atomic force microscope (AFM) in intermittent contact mode with a Nanoscope IIIa controller and an "E" scanner. Samples were prepared by an adaptation of the method reported by Sherratt et al. [24]. Briefly, hydrogels were diluted with $dH_2O$ to a concentration of 1 mmol/L (total peptide concentration), and 100 μL aliquot of the diluted solution was allowed to deposit onto a freshly cleaved mica surface (Agar Scientific, UK) for 60 s. Excess liquid was removed by capillary action and then the surface was rinsed twice with 500 μL of $dH_2O$ and left to air-dry overnight. For imaging, Olympus high aspect ratio etched silicon probes (Veeco, France) were used with spring constant of 42 N/m. Cantilever oscillation varied between 300 and 350 kHz, the drive amplitude was determined by the Nanoscope software, and height images were captured at a scan rate of 1.49 Hz with scan sizes of 5 or 2 $\mu m^2$. Height data was first-order flattened, and mean fibre widths were determined, using the software package WSxM. Correction for overestimation of lateral dimension due to tip geometry was performed as reported by Sherratt et al. [24], and widths at 3 points along 100 fibres were measured and averaged.

### 2.3. Transmission electron microscopy

The morphology of the self-assembled fibres was further assessed using a Tecnai 10 transmission electron microscope (TEM) operated at 100 keV using a reported protocol [23]. To prepare samples, carbon-coated copper grids (No. 400) were glow discharged for 5 s and placed shiny side down onto a 10 μL droplet of diluted hydrogel (total Fmoc-peptide concentration: 5 mmol/L) for <5 s. Loaded grids were immediately placed on a 10 μL droplet of $dH_2O$ for 60 s, and then stained with a 10 μL droplet of 4% (w/v) uranyl acetate for 60 s and blotted. Data were recorded onto Kodak SO-163 films and images were subsequently scanned using a UMAX2000 transmission scanner providing a specimen level increment of 3.66 Å/pixel. A crystallographic analysis suite (CRISP (Hovmoller)) was used to process and select a variety of scanned images with fibres of different lengths/widths. Selected individual fibres were CTF (contrast transfer function) corrected and fast Fourier transform (FFT) analysis was performed on cropped areas of 1024 × 1024 pixel boxes. Following tuning and zero scale adjustment, FFT was lattice filtered using an inverse filter with 5 pixel edge smoothing and then used to calculate a back projection of an averaged fibre section.

### 2.4. Circular dichroism

Information on Fmoc-peptide arrangements within the self-assembled fibrils was collected using circular dichroism (CD). To prepare samples, 0.5 mL of each hydrogel (total Fmoc-peptide concentration: 10 mmol/L) were pipetted into a cuvette and degassed. Data between wavelengths of 190–320 nm were collected with a bandwidth of 1 nm on a Jasco J-810 circular dichroism spectrometer. Temperature stability was controlled at 20 °C by a water circulator. The data were collected three times in the wavelength range and accumulated to obtain a single spectrum.

### 2.5. Fourier transform infrared spectroscopy

To supply complementary information on Fmoc-peptide arrangements, Fourier transform infrared (FTIR) spectra were obtained on a Nicolet 5700 FT-IR spectrophotometer accompanied with the Omnic software. A sample of each Fmoc-peptide hydrogel (total Fmoc-peptide concentration: 20 mmol/L) was placed onto a diamond ATR-accessory sample stage and excess water from the sample was absorbed by a filter paper (Whatman, UK). The samples were then scanned between the wavelengths of 4000 and 400 $cm^{-1}$ over 128 scans at an interval of 1.9285 $cm^{-1}$.

### 2.6. Fluorescence spectroscopy

Interactions between the fluorenyl-groups of the Fmoc-peptide molecules were investigated by fluorescence spectroscopy. 1.5 mL of each Fmoc-peptide solution (total peptide concentration: 20 mM) were pipetted into a 1.0 cm quartz cuvette and mixed with an equal volume of DMEM for gelation. Emission data of the self-assembled hydrogels were recorded on a Jasco FP-750 spectrofluorometer with a mixture of 1.5 mL $dH_2O$ and 1.5 mL DMEM as the background. Data between the wavelengths of 300 nm and 600 nm were collected with an excitation wavelength of 265 nm and bandwidth of 5 nm.

### 2.7. Rheometry

The visco-elasticity of the hydrogels was measured on a Bohlin C-VOR rheometer with a 20 mm/2° cone-plate geometry. The elastic and viscous moduli of the hydrogels were recorded as a function of frequency between 0.1 and 100 Hz. A solvent trap was used to keep the sample hydrated and an integrated temperature controller was used to maintain the temperature of the sample stage at 25 °C.

### 2.8. 3D-culture of human adult dermal fibroblasts

Human adult dermal fibroblasts (HDFa, Cascade, UK) were cultured in Dulbecco's Modified Eagle's Medium (DMEM, Gibco, UK) supplemented with 10% FCS (fetal calf serum, Gibco, UK) and 1% Antibiotic–Antimycotic solution (Gibco, UK). Prior to 3D-culture, cells within a sub-confluent monolayer were trypsinized using trypsin (0.05%)–EDTA·4Na (0.53 mM) solution (Gibco, UK) and resuspended in serum-free DMEM to obtain a cell concentration of $1 \times 10^6$ to$1 \times 10^7$/mL. Prior to preparation of the Fmoc-peptide solutions, the powders of Fmoc-FF, Fmoc-RGD and Fmoc-RGE were weighed into separate vials and sterilized by UV light for 30 min. The mixed Fmoc-FF/RGD solutions with the two Fmoc-peptides in various molar ratios were prepared as described in Section 2.1 and pre-warmed in a 37 °C/5% $CO_2$ incubator. The 100% Fmoc-FF and mixed Fmoc-FF/RGE solutions were prepared as controls following the same procedure and were also pre-warmed to 37 °C. To encapsulate HDFa cells, 100 μL aliquots of either Fmoc-peptide solution were pipetted into tissue culture inserts (Greiner Bio One, UK) placed in a 12-well plate and an equal volume

of cell suspension was pipetted into the solution-containing inserts. An immediate yet gentle shaking was applied to ensure the homogeneity of these mixtures. 2 mL aliquots of complete medium (DMEM plus 10% FCS and 1% Antibiotic–Antimycotic solution) were pipetted into the wells, and the 12-well plate was maintained in a 37 °C/5% $CO_2$ incubator. After 30 min an extra 200 μL of complete medium was placed on top of each cell-gel construct. The medium surrounding the inserts and on top of the constructs was changed 2 h post culture and then daily.

### 2.9. Live–dead assay

Viability of encapsulated cells was tested by a Live–Dead assay (Molecular Probes, UK) performed 3 h and then daily post culture. A 500 μL aliquot of the assay solution containing 4 μM EthD-1 (ethidium homodimer-1) and 2 μM calcein AM was pipetted onto each cell-gel construct. After 30-min incubation at room temperature, the constructs were mounted onto glass coverslips using Prolong™ gold antifade reagent (Invitrogen, UK) and observed using a Nikon Eclipse 50i fluorescence microscope with excitation filters of 494 nm (green, Calcein) and 528 nm (red, EthD-1).

### 2.10. F-actin staining

Morphology and F-actin arrangement of encapsulated cells were investigated with an FITC (fluorescein isothiocyanate) conjugated phalloidin staining assay (Sigma, UK). After 24 and 48 h in culture, cell-gel constructs were fixed in 4% (w/v) paraformaldehyde (Sigma–Aldrich, UK) for 30 min and permeabilized in 0.5% (v/v) Triton X-100 solution (Sigma–Aldrich, UK) in phosphate buffered saline (PBS, Gibco, UK) for 5 min. The samples were then soaked in FITC–phalloidin solution (50 μg/mL) for 24 h and counterstained with 1 μg/mL DAPI (Sigma–Aldrich, UK) in PBS for 1 h. Stained samples were mounted with Prolong™ Gold antifade reagent and observed using a Nikon Eclipse 50i fluorescence microscope with excitation filters of 495 nm (green, FITC) and 340 nm (blue, DAPI).

### 2.11. MTS assay

To quantify cell proliferation inside the cell-gel constructs, an MTS ((3-(4,5-dimethylthiazol-2-yl)-5-(3-carboxymethoxyphenyl)-2-(4-sulfophenyl)-2*H*-tetrazolium) salt in combination with electron coupling reagent PES (phenazine ethosulfate)) assay (Promega, UK) was performed at a series of time points. A 3D-culture standard was made by encapsulating cells into the Fmoc-peptide hydrogels following the above 3D-culture procedure and carrying out the assay (seeding concentrations for the standard specimen: $3.75 \times 10^6$ to $1.25 \times 10^7$/(mL of gel)). To perform the MTS assay, each cell-gel construct was transferred into a 24-well plate and incubated with 20% (v/v) MTS reagent in complete medium. The plates were then kept in the dark and shaken in a 37 °C orbital shaker for 2 h. Absorbance of the supernatants was measured by a LabSystems Ascent colorimetric plate reader at a wavelength of 492 nm.

### 2.12. Integrin blocking

To determine if cells were directly binding to the RGD sites via the α5β1 integrins, a blocking antibody was used. $2 \times 10^6$ HDFa cells in 980 μL serum-free DMEM were incubated with 20 μL of anti-human α5β1-integrin antibody (Chemicon, Millipore, UK) at 37 °C for 45 min. 100 μL aliquots of the cell–antibody mixture were then mixed with 100 μL aliquots of either Fmoc-FF/RGD or Fmoc-FF/RGE solutions in 12-well inserts. Normal cells with unblocked integrins encapsulated in the two hydrogels were set as comparisons (Cell density: $10^6$ cell/mL of gel). 2 mL complete medium were then added to soak each insert, with 200 μL extra placed onto the top of each cell-gel construct. After 20 h in culture, an F-actin staining assay was performed on the cell-gel constructs using the protocol described in Section 2.10.

## 3. Results and discussion

### 3.1. Hydrogel formation

Formation of the Fmoc-FF/RGD hydrogels utilizes the pH-sensitivity of the Fmoc-peptide self-assembly process. Previous work showed that Fmoc-FF (Fig. 1A) has low solubility at neutral pH but dissolves in alkali solutions; upon approaching pH 7, the Fmoc-FF molecules self-assemble and a macroscopic hydrogel is formed [9,23]. In contrast, Fmoc-RGD (Fig. 1A) dissolves in acid solutions and solutions of 10–20 mM Fmoc-RGD form transparent hydrogels at pH 3 at temperatures between 4 °C and 25 °C. Raising the temperature of the Fmoc-RGD hydrogels to 37 °C or applying mechanical forces (vortex or agitation) cause disassembly of the structure and dissolution of the gels, however the transparent gels can reform on standing at lower temperatures (4–20 °C), and the time for recovery depends on the agitation previously applied to the hydrogel and the temperature. To develop hydrogels that are both bioactive and stable under physiological conditions, solutions of Fmoc-FF (pH 10) and Fmoc-RGD (pH 3) in various volume ratios were mixed giving rise to translucent Fmoc-FF/RGD hydrogels containing 10–50 mM% Fmoc-RGD at 37 °C/pH 7.0 (Fig. 1B). Mixing DMEM into an equal volume of either Fmoc-FF/RGD solution at 37 °C can accelerate the molecular self-assembly, and in 1 min self-supporting hydrogels were observed to form. The metal ions within DMEM may play a role in this self-assembly acceleration as they screen charged residues in order to reduce molecular repulsion. This responsiveness of Fmoc-FF/RGD to culture medium provides a simple way to encapsulate cells for 3D culture, as cells suspended in culture medium can be mixed with the Fmoc-FF/RGD solutions to yield cell-gel constructs within 1 min.

### 3.2. Nanofibre morphology

A dried layer of the diluted Fmoc-FF/RGD hydrogels observed under AFM exposed an interwoven network of numerous nanofibres with bundles and entanglements, suggesting the existence of a three-dimensional nanofibrous structure within the hydrogels (a typical AFM height image of the nanofibre network is shown Fig. 1C). Morphology of individual nanofibres within the network was visualized by AFM and TEM, and as shown in Fig. 1C and D, the fibres observed for Fmoc-FF/RGD hydrogels appeared to be organized as 'flat ribbons' which were of heterogeneous widths and large aspect ratios. All Fmoc-FF/RGD hydrogels that contained 10–30 mM% Fmoc-RGD comprised nanofibres with this 'flat ribbon' appearance and this morphology resembled that previously observed for 100% Fmoc-FF (as shown in Supplementary data S7) [23]. Evidence for the inner structure of these 'flat-ribbons' was collected on a variety of the ribbons captured by TEM for each hydrogel. It was revealed that regular 'diffraction' spots with spacings of around 3 nm existed perpendicular to the length of the 'flat ribbons' (Fig. 1D inset). These 3 nm repetitions corresponded to the width of the fibrils which were organized parallel to each other within the ribbons; These 3 nm fibrils were also detected within the ribbons in 100% Fmoc-FF system, again implying the similarity between Fmoc-FF and mixed Fmoc-FF/RGD (with ≤30 mM% Fmoc-RGD) systems. When the Fmoc-RGD concentration was increased to >30% within the Fmoc-FF/RGD gels, nanofibres with regular twists along their length were observed by TEM and the mixed gels contained a mixture of twisted fibres and flat ribbons. When the hydrogel comprised 100% Fmoc-RGD molecules, all nanofibres within the structure possessed regular twists according to AFM and TEM (as shown in Supplementary data, S7). This twisted morphology might therefore reflect the molecular arrangement dominated by Fmoc-RGD, and was different from that observed in 100% Fmoc-FF or Fmoc-FF/RGD with ≤30% Fmoc-RGD, where the Fmoc-FF molecules dominated the self-assembly to form mixed Fmoc-FF/RGD fibres.

### 3.3. Molecular model

Using the information that both Fmoc-FF and Fmoc-FF/RGD (Fmoc-RGD: ≤30 mM%) contained similar flat ribbons that were composed of 3 nm wide fibrils, a molecular model for Fmoc-FF/RGD was proposed based on the hierarchical assembly of Fmoc-FF as previously reported [23]. This model was later verified by spectroscopic tests shown in Section 3.4. In the model (Fig. 1E), the two peptide sequences of FF and RGD self-assembled through intermolecular hydrogen bonds forming anti-parallel β-sheet structures. The Fmoc-groups on both peptides interacted with one another and formed π–π stacks to interlock the β-sheets. As a consequence of the inherent twisted nature of beta sheets [23], a cylindrical

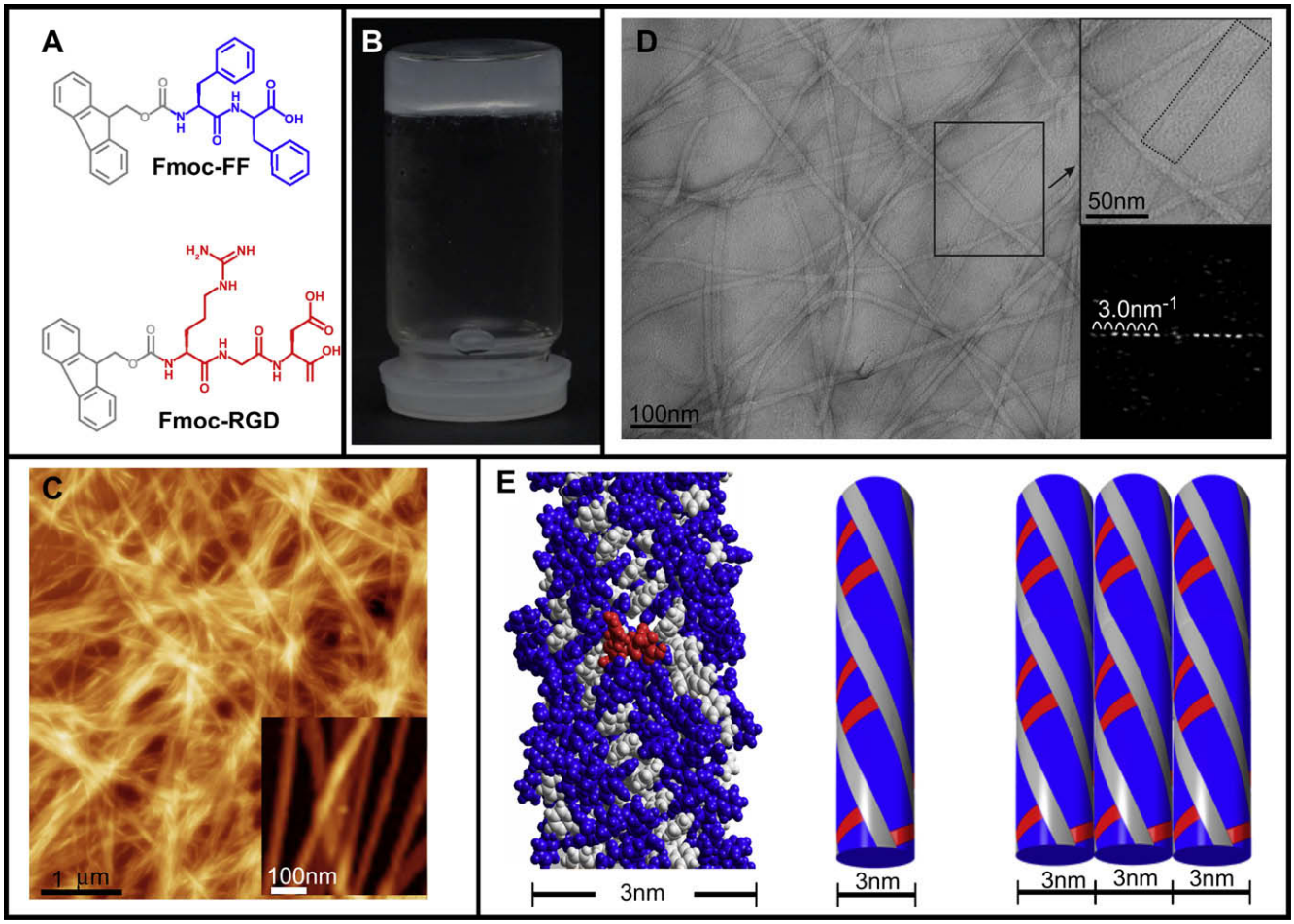


**Fig. 1.** The self-assembled hydrogel of Fmoc-FF/RGD, its nanofibrous structure and the supramolecular model. (A) The chemical structures of the hydrogel building blocks: Fmoc-FF and Fmoc-RGD. (B) The mixture of Fmoc-FF and Fmoc-RGD self-assembles into a translucent hydrogel at 37 °C. (C) The AFM height image of the hydrogel shows an overlapping mesh of nanofibres, with bundles and entanglements. (D) The TEM image shows that the nanofibres are 'flat ribbons' and they comprise parallel-aligned fine fibrils across their width. The fine fibrils have an average 3 nm diameter revealed by periodic repeats in reciprocal space (Fast Fourier Transform (FFT) analysis shown in the right corner of image D). (E) The proposed supramolecular model demonstrates the formation of the 3 nm fibrils and their further lateral assembly into larger ribbons. RGD sequences are presented on the fibre surface enhancing their accessibility and bio-availability.

structure of 3 nm in diameter was formed which further extended longitudinally into a supramolecular nano-fibril with RGD sequences presented at the fibril surface. These fibrils then aligned parallel to each other into larger 'flat-ribbons' until a stable structure was reached stopping the width expansion of these ribbons. As suggested by the model, the whole of the RGD sequences confined on the 3 nm wide fibril (thus the flat ribbon) surfaces may present high accessibility to the cells, and the bioactivity of these nanofibres was later verified as shown in Section 3.5.

### 3.4. Supramolecular arrangement

Spectroscopic tests were performed to verify the model. The CD spectra of the Fmoc-RGD, Fmoc-FF, and Fmoc-FF/RGD hydrogels (total peptide for each gel: 10 mmol/L) were collected between the wavelengths of 190 and 320 nm. For Fmoc-FF and Fmoc-FF/RGD (with Fmoc-RGD $\leq$30%), a broad negative peak was present at the wavelength of 218 nm, together with the spectra crossing the *x*-axis at 200 nm (Fig. 2A). This suggested that the peptides (FF or RGD) assembled into β-sheet structures. For 100% Fmoc-RGD, the negative peak between 210 and 230 nm was weak suggesting rare β-sheet structures were present compared to Fmoc-FF and Fmoc-FF/RGD with $\leq$30% Fmoc-RGD (Fig. 2A). For mixed gels with >30% Fmoc-RGD, the negative peak at 218 nm was replaced by a positive feature. This was probably due to the positive fluorenyl-peak interfering with the negative β-sheet peak; when relatively low amounts of β-sheets existed within the mixed gels (Fmoc-RGD >30%), the positive peak became dominant.

Complementary to CD, FTIR spectra were collected between the wavenumbers of 1400 and 1800 $cm^{-1}$ with the hydrogels prepared in $H_2O$ (Fig. 2B). For mixed gels with 10–30% Fmoc-RGD, two dominant peaks were located at the wavelengths of 1635 and 1691 $cm^{-1}$, suggesting that the main secondary structures were all antiparallel β-sheets confirming the results obtained by CD. This antiparallel β-sheets structure resembled that observed for 100% Fmoc-FF (Fig. 2B) thus confirmed the similarity of molecular arrangement for both systems. Additional peaks at 1656 and 1676 $cm^{-1}$ started to appear when the Fmoc-RGD concentration within the Fmoc-FF/RGD hydrogel increased to $\geq$30%, while for 100% Fmoc-RGD, the 1656 peak dominated (Fig. 2B), which indicated that a major proportion of random-coil structure existed [25].

The arrangements of fluorenyl groups in the supramolecular structures were followed by fluorescence emission spectroscopy for Fmoc-FF, Fmoc-RGD, and Fmoc-FF/RGD with 10–50% Fmoc-RGD. The total peptide concentration within each hydrogel was fixed at 10 mmol/L. The spectra were collected between wavelengths 300 and 600 nm with an excitation wavelength of 265 nm. A broad feature at around 450 nm was detected for the Fmoc-FF and the

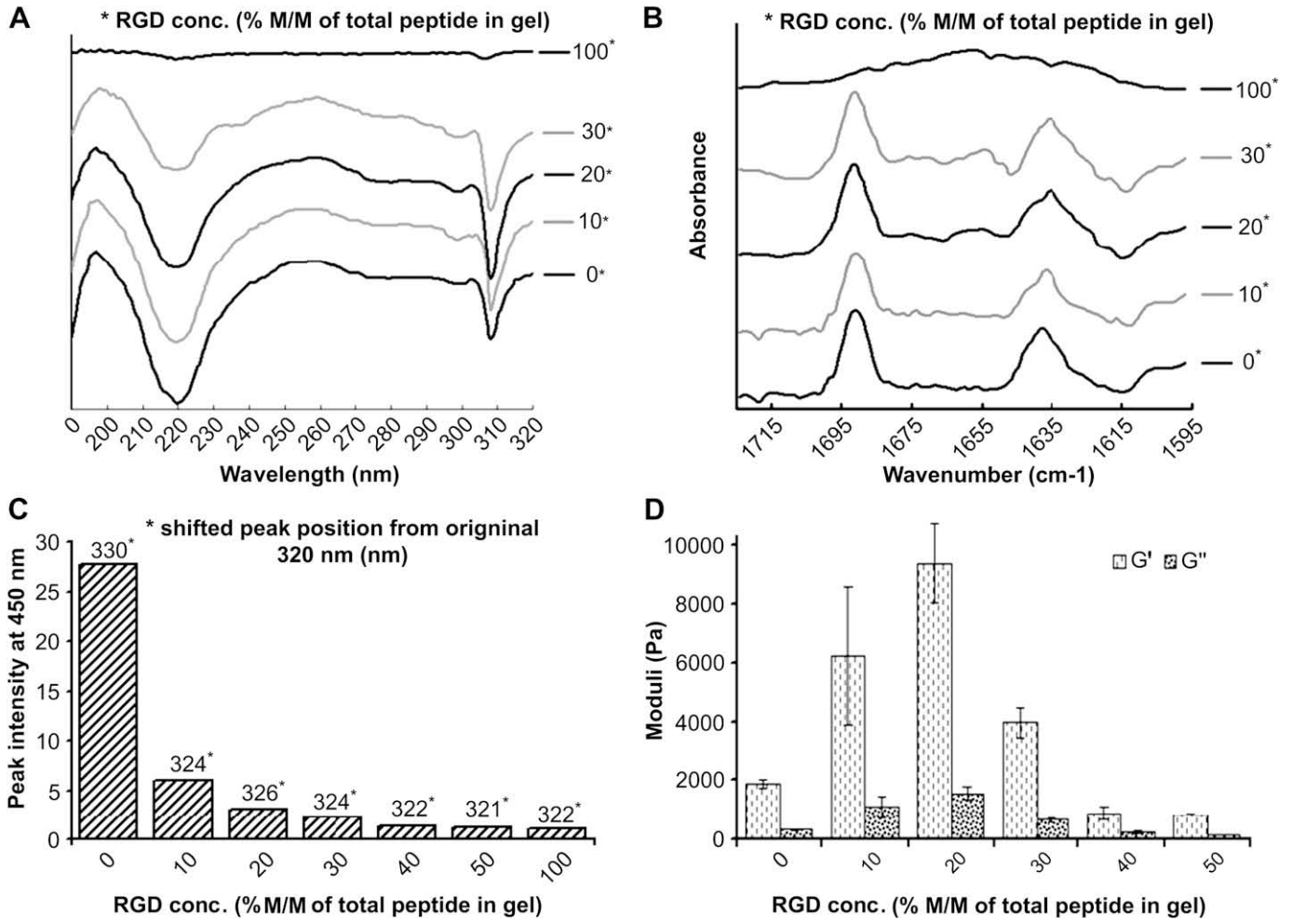


**Fig. 2.** Spectroscopic analyses and rheology of the self-assembled hydrogels. (A) CD spectra of the Fmoc-FF/RGD with 0–30% RGD show a broad negative peak at 218 nm suggesting formation of β-sheets. This peak is absent for the 100% Fmoc-RGD. (B) Two split peaks at around 1630 and 1690 $cm^{-1}$ are present on the FTIR spectra of the Fmoc-FF and Fmoc-FF/RGD hydrogels (with 0–30% RGD) suggesting the β-sheets are anti-parallel. For the 100% Fmoc-RGD, the two peaks are replaced by a broad peak at around 1655 $cm^{-1}$, indicative of random coil. (C) The fluorescence spectra (as shown in Supplementary data, S8) suggest that increasing the Fmoc-RGD concentration within 10–30% in the Fmoc-FF/RGD hydrogel (the total peptide concentration is fixed) decrease the intensity of the 450 nm peak which indicates subtle changes in fluorenyl interactions resulting in less extensive J-aggregates. (D) The Fmoc-RGD concentration influences the hydrogel visco-elasticity: The gradual increase of RGD mole fraction from 0% to 50% alters the elastic modulus ($G'$) of the hydrogel, however in a non-monotonic way.

Fmoc-FF/RGD gels (original spectra shown in Supplementary data, S8), which indicated the presence of extensive J-aggregates formed by the fluorenyl and phenyl rings through π–π interactions [26]. With the increase of the Fmoc-RGD component, the intensity of the 450 nm peak decreased (Fig. 2C), suggesting less effective π-stacking interactions. This was probably related to the fact that for 100% Fmoc-FF hydrogels, the relatively-high 450 nm peak corresponded to the J-aggregates consisted of heterogeneous stacks of phenyl rings (from the second phenylalanine residue) and fluorenyl rings, while the Fmoc-RGD molecules lack the terminal phenyl and therefore the mixed gels had a decreased 450 nm peak. However, when the Fmoc-FF molar fraction was kept constant (10 mmol/L) with increasing Fmoc-RGD (≤30%), the 450 peak continued to rise suggesting the interactions of Fmoc groups was regardless of the peptide attached to them, and Fmoc-groups of Fmoc-RGD were incorporated as regular stacks in the supramolecules (as shown in Supplementary data, S9). When the Fmoc-RGD component exceeded 30%, the intensity of the 450-nm peak dropped, and this peak virtually disappeared for the 100% Fmoc-RGD gel (as shown in Supplementary data, S9). In the spectra, peaks at 320 nm or slightly red-shifted towards 333 nm were also observed, presenting fluorenyl monomers and anti-parallel fluorenyl excimers [27,28]. This red-shift became smaller when more Fmoc-RGD was added. A 2 nm shift was detected for the 100% Fmoc-RGD suggesting the majority of the Fmoc-groups remained as un-assembled monomers. Overall, the above spectroscopic analyses suggested that at ≤30% Fmoc-RGD no significant disruption to the peptide interactions occurred although subtle changes in π-stacking interactions were detected.

### 3.5. Rheometry

Apart from the alteration in microscopic supramolecular structure, the Fmoc-RGD concentration also macroscopically influenced the visco-elasticity of the Fmoc-FF/RGD gels. Gels for rheometry analysis were prepared by mixing Fmoc-peptide solutions with an equal volume of DMEM. The resulting medium-containing hydrogels were rapid gelling and reflected the stiffness of the gels used in 3D-cell culture. In the oscillating rheometrical spectra collected for all the gels, the elastic modulus $G'$ appeared 4–7 times higher than the viscous modulus $G''$ indicating the systems were solid gels (as shown in Supplementary data, S10). The $G'$, as an indicator for hydrogel stiffness, changed with the increase of the Fmoc-RGD concentration yet in a non-monotonic way (Fig. 2D). With 10–30% Fmoc-RGD incorporated, the Fmoc-FF/RGD gels were stiffer than

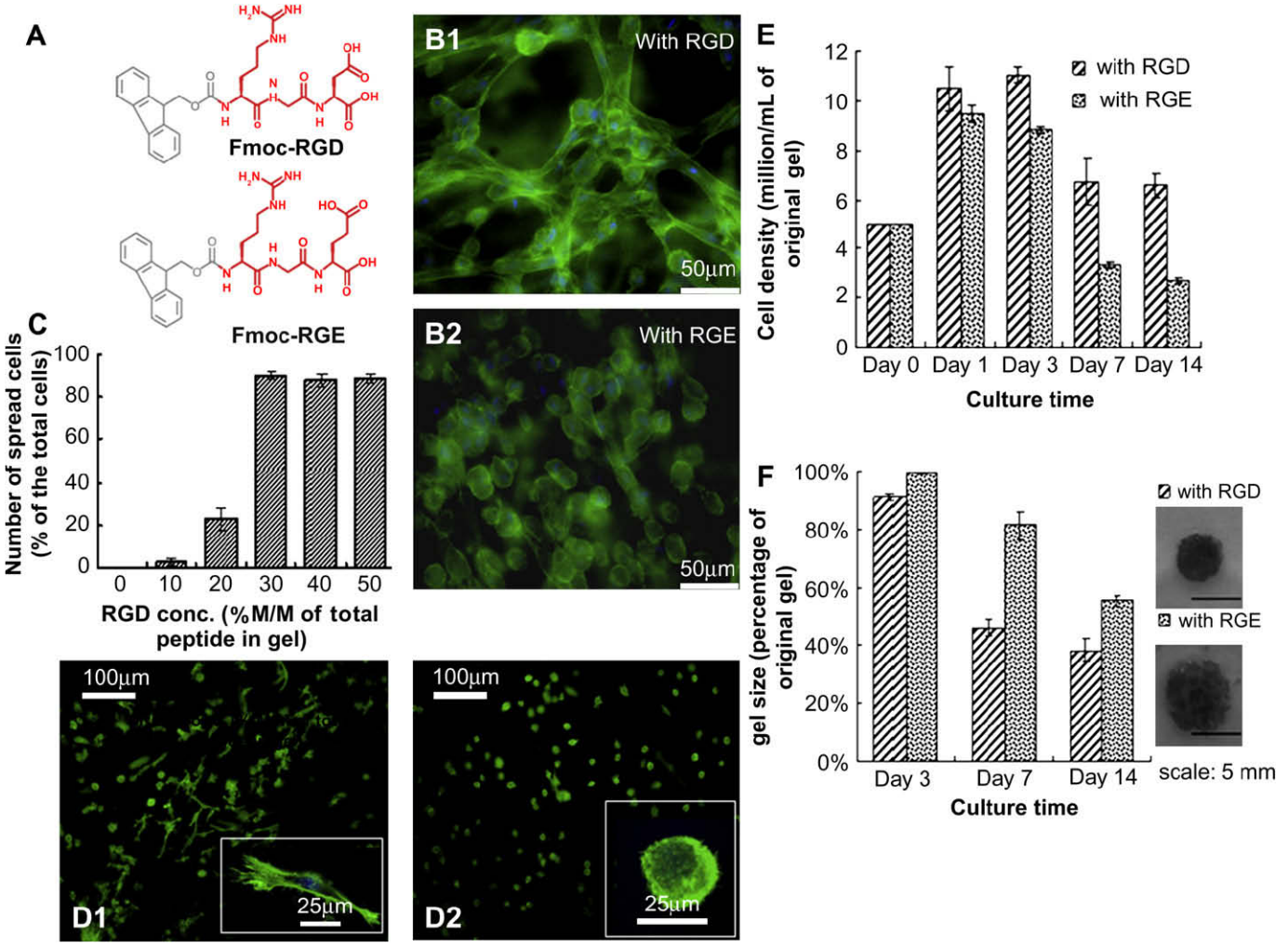


**Fig. 3.** The Fmoc-FF/RGD hydrogel promotes cell adhesion with subsequent cell spreading and proliferation. (A) The structures of the two chemical analogs: Fmoc-RGD and Fmoc-RGE. (B) Cell adhesion and morphology in the Fmoc-FF/RGD and Fmoc-FF/RGE hydrogels: human adult dermal fibroblasts (HDFa) are well-spread in the Fmoc-FF/RGD hydrogels, and form a three-dimensional cell network 48 h post culture (B1); HDFa in the Fmoc-FF/RGE hydrogels maintain a round morphology after 48 h (B2). (C) The Fmoc-RGD concentration also influenced cell spreading: in the hydrogels with 30–50% Fmoc-RGD incorporated, adequate cell spreading occurs with over 90% spread cells. (D) Integrin blocking experiments proved direct interaction of the cells with RGD after 20 h: Cells with unblocked α5β1 integrins were able to spread and directly attach to the RGD sites on the nanofibres (D1); Cells with blocked α5β1 integrins were unable to attach to the RGD sites and remained rounded (D2). (E) Cell proliferation in the Fmoc-FF/RGD and Fmoc-FF/RGE hydrogels: HDFa cells in Fmoc-FF/RGD undergo significant proliferation up to 3 days post culture. Between days 3 and 7 cell density started to decrease along with gradual gel contraction; however between days 7 and 14, cell density remained similar as gel size became stabilized. Final cell density was higher than the original culture density in Fmoc-FF/RGD. Cell number in Fmoc-FF/RGE decreased between days 1 and 3 and dropped lower than the original culture density by day 14. (F) Contraction of the cell-gel constructs: Fmoc-FF/RGD hydrogels contracted by approximately 60%, with the main contraction occurring between days 3 and 7. Fmoc-FF/RGE hydrogels contracted later, reducing their size to 45%.

the 100% Fmoc-FF ($G' \approx 1.9$ kPa) with their $G'$ ranging between 4 and 10 kPa; the gel with 20% Fmoc-RGD possessed the maximum $G'$ of 10 kPa which was higher than or comparable to other self-assembled hydrogel systems [8,14]. However, the gels with >30% RGD were softer ($G' \approx 0.8$–$0.9$ kPa) than the 100% Fmoc-FF. Combined with the spectroscopic data, these rheological data suggested that there are complex relationships between molecular composition, supramolecular organization and hydrogel characteristics; further understanding of the relationships may open up opportunities to match various hydrogels to specific cell types, as matrix stiffness may regulate cell morphology and differentiation as previously reported [29,30].

### 3.6. 3D culture and cell adhesion

The potential of these Fmoc-FF/RGD hydrogels as bioactive 3D-scaffolds for anchorage-dependent cells was then investigated. As a comparison, Fmoc-RGE (Fig. 3A) was chosen as a chemical analog and Fmoc-FF/RGE gels were prepared. To encapsulate HDFa (human adult dermal fibroblasts) cells into the hydrogels, a cell suspension in serum-free DMEM was mixed with an equal volume of either Fmoc-FF/RGD or Fmoc-FF/RGE solutions. The cell-gel constructs formed within 1 min at 37 °C, thus the homogeneity of the cell distribution was ensured throughout the hydrogels. The molecular self-assembly process did not affect cell viability according to a Live-Dead assay performed 3 h post culture. Living (green) cells with well-defined round contours were visualized and no dead cells (shown as red nuclei) were detected within the gels.

Within the first 24 h of culture, a cell-spreading process occurred in the Fmoc-FF/RGD (with 30–50% Fmoc-RGD) hydrogels, which suggested direct cell adhesion to the 3D-scaffold. The cells adopted a spindle or polyhedral shape with fine filopodia. After 48 h, the spread cells formed 3D-networks in the Fmoc-FF/RGD gels (Fig. 3B1); phalloidin-stained F-actin showed highly-elongated cells with clearly-defined stress fibres. Regular cell alignment was observed, possibly following aligned fibrous features of the

hydrogel. In contrast, cells in the Fmoc-FF/RGE gels maintained a spherical or ellipsoidal shape and phalloidin staining showed peripheral deposition of poorly organized F-actin that followed the cell contours (Fig. 3B2). The extent of cell spreading was influenced by the Fmoc-RGD concentration within the Fmoc-FF/RGD hydrogels (Fig. 3C). Approximately 90% of the cells were spread within the gels which contained $\geq$30% RGD; the percentage of spread cells dropped to under 50% when $\leq$20% RGD was incorporated. Cells maintained a round morphology in the gels with 0–10% RGD.

### 3.7. RGD–integrin binding

To determine whether the cells were directly binding to the RGD sequence via their RGD–integrin ($\alpha5\beta1$), a blocking antibody was used. Prior to 3D-culture, cells were incubated with JBS5—an $\alpha5\beta1$-integrin blocking antibody. These cells were then encapsulated into the hydrogels. Cells with unblocked integrins were observed to spread in the Fmoc-FF/RGD gels within 24 h with reorganized cytoskeletal F-actin filaments (Fig. 3D1), whereas the cells with blocked $\alpha5\beta1$ integrins lost their ability to recognize the extracellular RGD-ligands on the self-assembled nanofibre surface, and failed to attach and spread (Fig. 3D2). As expected, the $\alpha5\beta1$ integrins had no influence on cell adhesion to the Fmoc-FF/RGE hydrogels; whether or not their integrins were blocked, the cells remained rounded with disorganized F-actin similar to cells in suspension (as shown in Supplementary data, S11). This observation therefore suggested the fibronectin integrin $\alpha5\beta1$ acted as a mediator linking cells to the Fmoc-FF/RGD matrix.

### 3.8. Cell proliferation and gel contraction

Proliferation of the HDFa cells in the Fmoc-FF/RGD hydrogels was followed by a quantitative MTS assay for 14 days (Fig. 3E). The RGD concentration was chosen at 30% as this yielded a gel which possessed relatively high stiffness and still promoted 90% cell-spreading. With the process of cell adhesion and spreading in the Fmoc-FF/RGD gels, number of metabolically-active cells was continuously increasing during the initial 3-day culture. Contraction of the cell-gel constructs then occurred, and the number of metabolically-active cells decreased with it. This phenomenon persisted until day 7 when construct contraction was significantly slowed, and cell number remained similar between days 7 and 14. The final cell density for the Fmoc-FF/RGD was 30% higher than the original culture density. In the Fmoc-FF/RGE gels, cell number started to decrease between days 1 and 3 due to the lack of cell attachment, and this continued up to day 14 with a final cell density 46% lower than the initial cell density (Fig. 3E).

Both the Fmoc-FF/RGD and the Fmoc-FF/RGE hydrogels underwent contraction (Fig. 3F), with the Fmoc-FF/RGD gels contracting to a greater extent. The final hydrogels were 38% of the original size for the Fmoc-FF/RGD, compared to 55% for the Fmoc-FF/RGE. The major contraction of the Fmoc-FF/RGD occurred between days 3 and 7, and the contraction was significantly slowed between days 7 and 14 when cell number reached a plateau. For the Fmoc-FF/RGE, the contraction started later and continued steadily up to day 14. The greater contraction of the Fmoc-FF/RGD gels suggested that when spread cells formed a 3D network between day 1 and day 3, cells pulled the nanofibres that they had adhered to and remodeled the extracellular fibrous matrix—a phenomenon similar to wound contraction *in vivo* [31].

## 4. Conclusions

In summary, by following a minimalist approach, self-assembled bioactive hydrogels composed of simple Fmoc-FF and Fmoc-RGD were developed to successfully culture human dermal fibroblasts three-dimensionally *in vitro*. The unique molecular structure of the nanofibres allowed the complete presence of the RGD sequences at the fibre surface with their conformation stabilized by the hydrogen bonds with neighboring peptide sequences. These simple small-molecule hydrogels have great potential as cost-effective model scaffolds for the 3D-culture of other anchorage-dependent cells. The study of cells within a 3D environment rather than the common 2D substrate will lead to advances in areas such as cell therapy, tissue engineering and fundamental cell biology. Based on the current self-assembled systems of Fmoc-FF/RGD, possibilities of recruiting other bioactive ligands into these systems exist (such as the synergistic sequence PHSRN [32] and other peptides) to enhance the effects of RGD or supply other bio-functions for the fulfillment of other requirements in biology.

## Acknowledgements

The authors thank Johnson & Johnson Wound Management (Gargrave, UK) for the financial support of Mi Zhou, and the EPSRC and Leverhulme Trust for financial support of Andrew Smith and Apurba Das. Nigel Hodson acknowledges the support of the UK Centre for Tissue Regeneration (a partnership between NorthWest Development Agency and University of Manchester, UK).

## Appendix

Figures with essential colour discrimination. Certain figures in this article, in particular parts of Figs. 1 and 3 are difficult to interpret in black and white. The full colour images can be found in the online version, at doi:10.1016/j.biomaterials.2009.01.010.

## Appendix. Supplementary data

Supplementary data associated with this article can be found in the online version at doi:10.1016/j.biomaterials.2009.01.010.

## References

[1] Alberts B, Bray D, Hopkin K, Johnson A, Lewis J, Raff M, et al. Tissues and cancer. In: Essential cell biology. New York & London: Garland Science Press; 2004. p. 697–738.
[2] Zhang S. Fabrication of novel biomaterials through molecular self-assembly. Nat Biotechnol 2003;21:1171–8.
[3] Mart RJ, Osborne RD, Stevens MM, Ulijn RV. Peptide-based stimuli-responsive biomaterials. Soft Mater 2006;2:822–35.
[4] Zhang S, Holmes TC, Dipersio GM, Hynes RO, Su X, Rich A. Self-complementary oligopeptides matrices support mammalian cell attachment. Biomaterials 1995;16:1385–93.
[5] Kisiday J, Jin M, Kurz B, Hung H, Semino C, Zhang S, et al. Self-assembling peptide hydrogel fosters chondrocyte extracellular matrix production and cell division: implications for cartilage tissue repair. Proc Natl Acad Sci U S A 2002;99:9996–10001.
[6] Hartgerink JD, Beniash E, Stupp SI. Peptide-amphiphile nanofibres: a versatile scaffold for the preparation of self-assembling materials. Proc Natl Acad Sci U S A 2002;99:5133–8.
[7] Beniash E, Hartgerink JD, Storrie H, Stendahl JC, Stupp SI. Self-assembling peptide amphiphile nanofibre matrices for cell entrapment. Acta Biomater 2005;1:387–97.
[8] Kretsinger JK, Haines LA, Ozbas B, Pochan DJ, Schneider JP. Cytocompatibility of self-assembled β-hairpin peptide hydrogel surfaces. Biomaterials 2005;26:5177–86.
[9] Jayawarna V, Ali M, Jowitt TA, Miller AF, Saiani A, Gough JE, et al. Nanostructured hydrogels for three-dimensional cell culture through self-assembly of fluorenylmethoxycarbonyl-dipeptides. Adv Mater 2006;18:611–4.
[10] Haines-Butterick L, Rajagopal K, Branco M, Salick D, Rughani R, Pilarz M, et al. Controlling hydrogelation kinetics by peptide design for three-dimensional encapsulation and injectable delivery of cells. Proc Natl Acad Sci U S A 2007;104:7791–6.
[11] Silva GA, Czeisler C, Niece KL, Beniash E, Harrington DA, Kessler JA, et al. Selective differentiation of neural progenitor cells by high-epitope density nanofibres. Science 2004;303:1352–5.

[12] Guler MO, Hsu L, Soukasene S, Harrington DA, Hulvat JF, Stupp SI. Presentation of RGD epitopes on self-assembled nanofibres of branched peptide amphiphiles. Biomacromolecules 2006;7:1855–63.
[13] Rajangam K, Behanna HA, Hui MJ, Han X, Hulvat JF, Lomasney JW, et al. Heparin binding nanostructures to promote growth of blood vessels. Nano Lett 2006;6:2086–90.
[14] Storrie H, Guler MO, Abu-Amara SN, Volberg T, Rao M, Geiger B, et al. Supramolecular crafting of cell adhesion. Biomaterials 2007;28:4608–18.
[15] Pierschbacher MD, Ruoslahti E. Cell attachment activity of fibronectin can be duplicated by small synthetic fragments of the molecule. Nature 1984;309:30–3.
[16] Lutolf MP, Hubbell JA. Synthetic biomaterials as instructive extracellular microenvironments for morphogenesis in tissue engineering. Nat Biotechnol 2005;23:47–55.
[17] Hern DL, Hubbell JA. Incorporation of adhesion peptides into nonadhesive hydrogels useful for tissue resurfacing. J Biomed Mater Res 1998;39:266–76.
[18] Hersel U, Dahmen C, Kessler H. RGD modified polymers: biomaterials for stimulated cell adhesion and beyond. Biomaterials 2003;24:4385–415.
[19] Gras SL, Tickler AK, Squires AM, Devlin GL, Horton MA, Dobson CM, et al. Functionalized amyloid fibrils for roles in cell adhesion. Biomaterials 2008;29:1553–62.
[20] Massia SP, Hubbell JA. An RGD spacing of 440 nm is sufficient for integrin $\alpha_v\beta_3$-mediated fibroblast spreading and 140 nm for focal contact and stress fibre formation. J Cell Biochem 1991;114:1089–100.
[21] Cavalcanti-Adam EA, Micoulet A, Blummel J, Auernheimer J, Kessler H, Spatz JP. Lateral spacing of integrin ligands influence cell spreading and focal adhesion assembly. Eur J Cell Biol 2006;85:219–24.
[22] Maheshwari G, Brown G, Lauffenburger DA, Wells A, Griffith LG. Cell adhesion and motility depend on nanoscale RGD clustering. J Cell Sci 2000;113:1677–86.
[23] Smith AM, Williams RJ, Tang C, Coppo P, Collins RF, Turner ML, et al. Fmoc-diphenylalanine self-assembles to a hydrogel via a novel architecture based on $\pi$–$\pi$ interlocked $\beta$-sheets. Adv Mater 2008;20:37–41.
[24] Sherratt MJ, Bax DV, Chaudhry SS, Hodson NW, Lu JR, Saravanapavan P, et al. Substrate chemistry influences the morphology and biological function of adsorbed extracellular matrix assemblies. Biomaterials 2005;26:7192–206.
[25] Goormaghtigh E, Cabiaux V, Ruysschaert JM. Determination of soluble and membrane protein structure by Fourier transform infrared spectroscopy. III. Secondary structures. Subcell Biochem 1994;23:405–50.
[26] Song B, Wei H, Wang Z, Zhang X, Smet M, Dehaen W. Supramolecular nanofibres by self-organization of bola-amphiphiles through combination of hydrogen bonding and pi–pi stacking interaction. Adv Mater 2007;19:416–20.
[27] Yang Z, Gu H, Zhang Y, Wang L, Xu B. Small molecule hydrogels based on a class of anti-inflammatory agents. Chem Commun 2004:208–9.
[28] Pinion JP, Minn FL, Filipescu N. Excimer emission from dibenzofuran and substituted fluorenes. J Lumin 1971;3:245–52.
[29] Tomasek JJ, Gabbiani G, Hinz B, Chaponnier C, Brown RA. Myofibroblasts and mechano-regulation of connective tissue remodelling. Nat Rev Mol Cell Biol 2002;3:349–63.
[30] Engler AJ, Sen S, Sweeney HL, Discher DE. Matrix elasticity directs stem cell lineage specification. Cell 2006;126:677–89.
[31] Stadelmann WK. Physiology and healing dynamics of chronic cutaneous wounds. Am J Surg 1998;176:26–38.
[32] Aota S, Nomizu M, Yamada KM. The short amino acid sequence Pro-His-Ser-Arg-Asn in human fibronectin enhances cell-adhesive function. J Biol Chem 1994;269:24756–61.